Computationally-Guided Catalyst Design in the Type I Dynamic Kinetic Asymmetric Pauson–Khand Reaction of Allenyl Acetates

Lauren C. Burrows, Luke T. Jesikiewicz, Gang Lu, Steven J. Geib, Peng Liu*, Kay M. Brummond*

Department of Chemistry, University of Pittsburgh, Pittsburgh, Pennsylvania 15260

ABSTRACT: The Rh(I)-catalyzed allenic Pauson–Khand reaction (APKR) is an efficient, redox-neutral method of synthesizing α-acyloxy cyclopentenones. An enantioselective APKR could provide access to chiral, non-racemic α-acyloxy and α-hydroxy cyclopentenones and their corresponding redox derivatives, such as thapsigargin, a cytotoxic natural product with potent antitumor activity. Rapid scrambling of axial chirality of allenyl acetates in the presence of Rh(I) catalysts enables the conversion of racemic allene to enantiopure cyclopentenone product in a dynamic kinetic asymmetric transformation (DyKAT). A combined experimental and computational approach was taken to develop an effective catalytic system to achieve the asymmetric transformation. The optimization of the denticity, and steric and electronic properties of the ancillary ligands identified a hemilabile bidentate (*S*)-MonoPhos-alkene Rh(I) catalyst that provided α-acyloxy cyclopentenone product in high er. Enantioselectivity was rationalized using ligand-substrate steric interactions and distortion energies in the computed transition states. This asymmetric APKR of allenyl acetates is a rare example of a Type I DyKAT reaction of an allene, the first example of DyKAT in a cyclocarbonylation reaction, and the first catalyst-controlled enantioselective APKR.

INTRODUCTION

An ultimate challenge in synthesis is the development of methods to prepare enantioenriched compounds. α-Acyloxy[1] and α-hydroxy[2] cyclopentenones, and their corresponding redox derivatives,[3] appear in numerous natural products, but enantioselective access to these functional group arrays is limited. α-Oxygenated ketones are typically prepared via the installation of a hydroxyl group adjacent to an existing carbonyl.[4] However, there are only a few methods for the asymmetric preparation of these groups using this strategy, and stereoselectivity in these cases is substrate- or reagent-controlled.[5] An enantioselective method where either enantiomer of an α-acyloxy ketone could be accessed with catalyst-controlled selectivity would be a valuable addition to the toolbox of asymmetric synthesis.[6]

The allenic Pauson-Khand reaction (APKR) of allenyl acetates, catalyzed by Rh biscarbonyl chloride dimer ([Rh(CO)$_2$Cl]$_2$), is an efficient method of synthesizing α-acyloxy cyclopentenones, and its utility for the preparation of highly oxygenated ring systems has been demonstrated (Figure 1A).[7] In addition, the APKR offers a redox economical approach to bicyclo[5.3.0]decane ring structures prevalent in 6,12-guaianolides[8] such as thapsigargin (Tg, **3a**, Figure 1B)[9a-d, 10, 11] and Mipsagargin (**3b**),[9e] and other polycyclic natural products.[12] During studies to explore the scope of the APKR of allenyl acetates, we observed the formation of **2** in 76% yield.[7] Surprisingly, the diastereoselectivity for the formation of **2** was 2:1, even though the allene-yne **1** was a 1:1 mixture of diastereomers. Subjecting a 5:1 dr of product **2** to the APKR reaction conditions showed the same dr after 24 h. Subjecting a 3:1 mixture of allenyl acetates to the APKR reaction conditions for 40 min at 90 °C or at rt for 7 h resulted in a 1:1 ratio of diastereomers with no evidence of APKR product **2**.

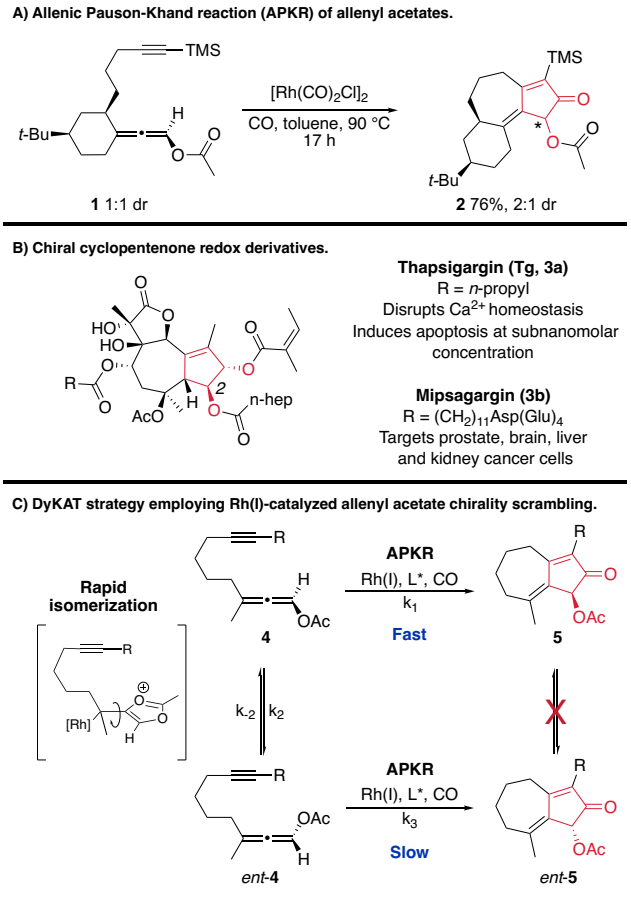

Figure 1. APKR of allenyl acetates to access chiral non-racemic α-acyloxy cyclopentenones.

Finally, no scrambling of axial chirality was observed in the absence of the Rh(I) catalyst. These observations suggested the potential for a Type I dynamic kinetic asymmetric transformation (DyKAT) where racemic allenyl acetate **4** could be converted to a single enantiomer of the product **5** via the rapid scrambling of the axial chirality of the allene (k_2, k_{-2}) and the selective APKR of one allene enantiomer ($k_1 > k_3$, or $k_3 > k_1$) when using a chiral Rh(I) catalyst (Figure 1C).[13]

Impressive advancements have been made in the enantioselective Rh-catalyzed Pauson-Khand reactions (PKR) of enynes, including development of room temperature conditions,[14] using aldehydes as a carbon monoxide replacement,[15] and catalyst immobilization.[16] However, the scope of the enantioselective Rh-catalyzed PKR has been limited to only 1,6-enyne substrates.[17] If successful, this work would represent a rare example of a DyKAT reaction of an allene,[18] the first example of DyKAT in a cyclocarbonylation reaction, and the first catalyst-controlled enantioselective APKR. Thus, we set out to test the feasibility of the asymmetric APKR to prepare enantioenriched α-acyloxy cyclopentenones.

A combination of theory and experiment was used to identify a chiral Rh(I) catalyst to effect this asymmetric transformation from racemic allenes. We utilized a rational catalyst design process that relied on computational insights with experimental validation, rather than experimentally screening a large number of chiral ligands.[19] This process comprised three steps: (1) experimentally identifying a suitable ligand class affording the APKR product in high yield with some enantioselectivity, (2) elucidating the APKR mechanism involving that ligand class using density functional theory (DFT) calculations to establish the enantioselectivity-determining step, and (3) using an iterative feedback loop involving rational selection of a ligand based on DFT calculations and experimental observation, and testing the performance of the ligand both experimentally and computationally (Figure 2). Although computation is often used to study reaction mechanisms and explain experimental results, development of the tools required to design catalysts *in silico* is still in its infancy.[20] Computational predictions involving transition metal catalysts for asymmetric transformations are especially challenging because a number of factors need to be considered, such as reactivity, regio- and stereoselectivity, catalyst stability, and side- and background-reactions. We hypothesized that the efficacy and reliability of the computational predictions could be improved by using the three-step approach described in the present study. Using this strategy, a DyKAT-based asymmetric APKR was efficiently developed using a practical balance of computational and experimental resources.

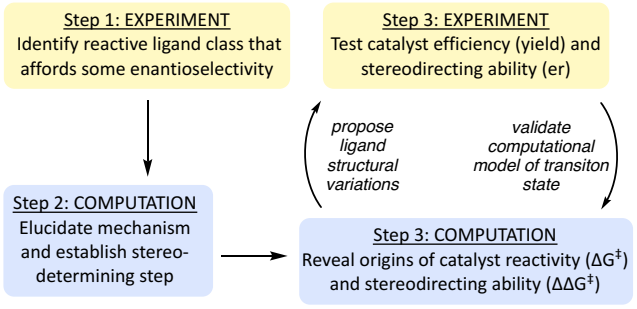

Figure 2. A synergistic strategy for catalyst design.

RESULTS AND DISCUSSION

Preparation of racemic allenyl acetates 9a-f. Methyl ketones **6a** and **6b** were prepared in three steps from 5-hexen-1-ol (see Supporting Information, SI). Trimethylsilyl (TMS)-alkyne **6c** was synthesized in four steps from 4-pentyn-1-ol, as previously reported.[7] Propargyl acetates **7a-c** were synthesized in one step from methyl ketones **6a-c** by addition of ethynylmagnesium bromide, followed by acetyl chloride (Conditions A, Scheme 1A). Propargyl pivalate **7d**, octanoate **7e**, benzoate **7f**, and *p*-nitrobenzoate **7g** were prepared from TMS-methyl ketone **6c** in two steps. Addition of ethynylmagnesium bromide followed by aqueous workup (Conditions B) provided propargyl alcohol **8c** in 88% yield. Propargyl pivalate **7d** was synthesized by reacting propargyl alcohol **8c** and pivalic anhydride with catalytic scandium(III) trifluoromethanesulfonate in 86% yield (Conditions C). Propargyl octanoate **7e** was prepared in 45% yield by reacting alcohol **8c** with octanoic acid, *N*,*N*'-dicyclohexylcarbodiimide (DCC) and 4-dimethyl aminopyridine (DMAP, Conditions D). Propargyl benzoate **7f** was prepared in 55% yield from propargyl alcohol **8c** using benzoic anhydride, triethylamine, and DMAP (Conditions E). *P*-nitrobenzoyl chloride, and DMAP were reacted with propargyl alcohol **8c** to afford **7g** in 84% yield (Conditions F). Propargyl acetates **7a-g** were reacted with Rh(II) bistrifluoroacetate dimer ($[Rh(OCOCF_3)_2]_2$) to afford the allenes **9a-g** in high yields (77-94%).

Scheme 1. Synthesis of allenyl acetates and racemic APKR.

A) Synthesis of allenyl acetates 9a-g from methyl ketones 6a-c.

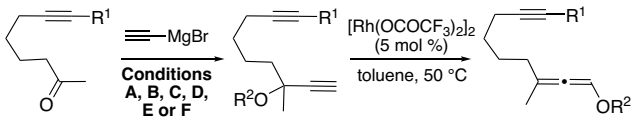

6a R^1 = Ph
6b R^1 = TIPS
6c R^1 = TMS

7a R^1 = Ph, R^2 = Ac, 65%
7b R^1 = TIPS, R^2 = Ac, 62%
7c R^1 = TMS, R^2 = Ac, 71%
8c R^1 = TMS, R^2 = H, 88%
7d R^1 = TMS, R^2 = Piv, 86%
7e R^1 = TMS, R^2 = $CO(CH_2)_6CH_3$, 45%
7f R^1 = TMS, R^2 = Bz, 55%
7g R^1 = TMS, R^2 = PNB, 84%

9a 91%
9b 94%
9c 93%
9d 89%
9e 77%
9f 87%
9g 89%

Conditions A: AcCl, **B:** NH_4Cl (sat'd aq), **C:** $Sc(OTf)_3$ (5 mol %), Piv_2O, **D:** octanoic acid, DCC, DMAP **E:** NEt_3, DMAP, Bz_2O, **F**: *p*-NO_2-C_6H_4COCl, DMAP, pyridine

B) Reaction of allene-ynes 9a-c under cationic and neutral Rh(I) conditions.

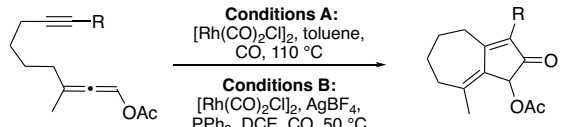

9a R = Ph
9b R = TIPS
9c R = TMS

	A	B
10a R = Ph	30%	61%
10b R = TIPS	50%	16%
10c R = TMS	47%	70%

Identification of catalyst and substrate for asymmetric APKR studies. To identify a preliminary reaction model system for DyKAT optimization, three allene-ynes **9a-c**, with different substituents at the alkyne terminus were reacted under neutral and cationic Rh(I) conditions (Conditions A and B, respectively, Scheme 1B). The reaction of phenyl-substituted alkyne **9a** gave **10a** in 30% and 61% yield, the triisopropylsilyl (TIPS)-alkyne **9b** afforded **10b** in 50 and 16% yield, and the trimethylsilyl (TMS)-substituted alkyne **9c** afforded **10c** in 47 and 70% yield, respective-

ly. Because allene-yne **9c** gave the highest yield under the cationic Rh(I) conditions in the presence of a phosphine ligand at lower temperature (50 versus 110 °C), we focused on the APKR of **9c** using cationic Rh catalysts in the development of the asymmetric catalytic system.

Identification of an effective ligand class for asymmetric APKR. Several types of chiral ligands have been successfully used in the asymmetric PKR of enynes.[21] We evaluated the effectiveness of select ligands of these types in the reaction of allene-yne **9c** (Table 1). Initial studies with chiral bidentate phosphines gave low yields and no enantioselectivity. For example, reaction with (*R*)-BINAP (**L1**) and $AgBF_4$ afforded a 13% yield of **10c** with a 50:50 enantiomeric ratio (er) and (*R*)- MeO-BIPHEP (**L2**) and $AgBF_4$ afforded a 21% yield of **10c** with a 51:49 er (Table 1, entries 1 and 2).[22] Both bisphosphine ligands **L1** and **L2** afforded aldehyde **11c** as the major product.[23] Catalyst Rh(IMes **L3**)(cod)Cl (cod = 1,5-cycloocta-diene) with the strongly electron donating *N*-heterocyclic carbene (NHC) ligand was unreactive in the APKR and afforded only unreacted starting material (Table 1, entry 3).[24] The poor yields observed in these initial experiments prompted us to test less sterically demanding and less σ-donating ligands. To this end, monodentate phosphoramidite ligand (*S*)-MonoPhos (**L4**) provided **10c** in 76% yield with a 58:42 er (Table 1, entry 4). Identification of monodentate phosphoramidites as an effective ligand class for the asymmetric APKR inspired a thorough examination of the APKR mechanism in order to discover ligand structural modifications to improve enantioselectivity.

Table 1. Experimental screening of ligand classes in the APKR of 9c.

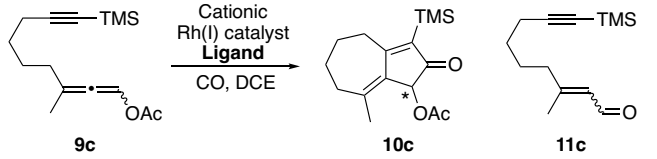

9c **10c** **11c**

entry	Ligand	T (°C)	time (h)	yield (%) 10c	11c	er [a]
1	**L1** [b]	90	16	13	18	50:50
2	**L2** [c]	80	5	21	28	51:49
3	**L3** [d]	50	15	0 [e]	0	-
4	**L4** [f]	50	5	76	5	58:42

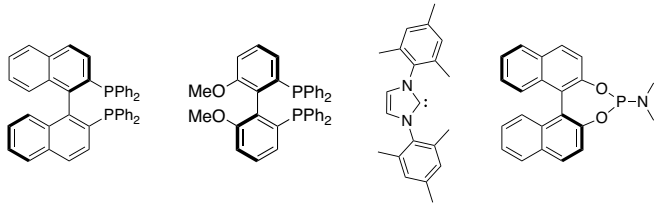

(*R*)-BINAP (**L1**) (*R*)-MeO-BIPHEP (**L2**) IMes (**L3**) (*S*)-MonoPhos (**L4**)

[a] Enantiomeric ratios were determined by HPLC using a chiral stationary phase. [b] $[Rh(CO)_2Cl]_2$ (10 mol %), **L1** (22 mol %), $AgBF_4$ (20 mol %), DCE, CO (1 atm). [c] $[Rh(CO)_2Cl]_2$ (10 mol %), **L2** (22 mol %), $AgBF_4$ (20 mol %), DCE, CO (1 atm) [d] [Rh(IMes **L3**)(cod)(Cl)] (10 mol %), $AgBF_4$ (10 mol%) DCE, CO (1 atm). [e] Recovered starting material. [f] $Rh(cod)_2BF_4$ (10 mol %), **L4** (15 mol %), DCE, CO (1 atm).

Calculation of the APKR mechanism and the enantioselectivity-determining transition state. After the experimental identification of monodentate phosphoramidites as an effective ligand class, DFT calculations were performed to determine the mechanism and the enantio-determining transition state geometry of the APKR using the Rh(I)-(*S*)-MonoPhos (**L4**) catalyst. With this information, we could evaluate how the structural modification of (*S*)-MonoPhos (**L4**) would improve enantioselectivity while maintaining good catalytic activity. Several previous computational studies of Co-catalyzed PKRs have been reported,[25] as well as a DFT study of a diastereoselective Rh-catalyzed PKR of an enyne.[26] In collaboration with Jordan, one of our groups has reported a rationalization for the metal-dependent regioselectivity of Rh(I)- and Mo(0)-catalyzed APKRs using DFT calculations.[27] However, all of the previous computational studies on the Rh-catalyzed PKR reactions were performed using $Rh(CO)_nCl$ or $Rh(CO)_n^+$ as the active catalyst (n = 1 or 2). The mechanism of PKR using other Rh(I) catalysts and the effects of ligands on reactivity and enantioselectivity have not been investigated computationally.

The accepted mechanism of the Rh-catalyzed APKR is illustrated in Scheme 2.[27] Coordination of allene-yne **II** to the catalyst **I** affords complex **III**, which undergoes oxidative cyclization to afford Rh(III) intermediate **IV.** Subsequent CO insertion, followed by reductive elimination and product dissociation provides cyclopentenone product **VII**.

Scheme 2. Accepted mechanism of the Rh(I)-catalyzed APKR.

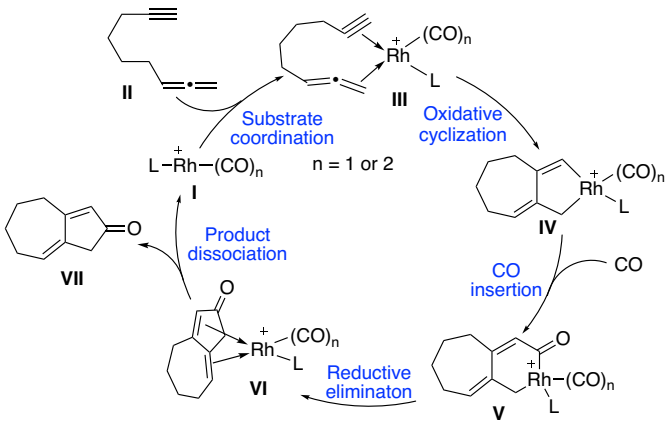

The computed reaction energy profiles of the cationic Rh-(*S*)-MonoPhos (**L4**)-catalyzed APKR with (*R*)-**9c** are shown in Scheme 3. We considered two different oxidative cyclization pathways with active Rh catalysts bearing either one or two CO ligands. In each pathway, only the energies of the most stable isomers are shown. The less stable isomers of the oxidative cyclization transition states and the different reactivities of (*R*)- and (*S*)-**9c** are discussed in detail later. The calculations were performed using B3LYP/6-31G(d)–LANL2DZ(Rh) for geometry optimizations and M06/6-311+G(d,p)–SDD(Rh) /SMD (DCE) for single point energy calculations (see SI for computational details). In both pathways, the resting state of the catalyst is the square-planar complex **12**. Coordination of allene-yne **9c** to replace two CO ligands in **12** requires 5.5 kcal/mol to afford substrate complex **13**, in which both the alkyne and allene π bonds are coordinated to the Rh center. Subsequent oxidative cyclization of complex **13** via **14-TS** requires an activation free energy of 21.9 kcal/mol with res-

Scheme 3. Computed reaction energy profile of the cationic Rh-(*S*)-MonoPhos (L4)-catalyzed APKR.[a]

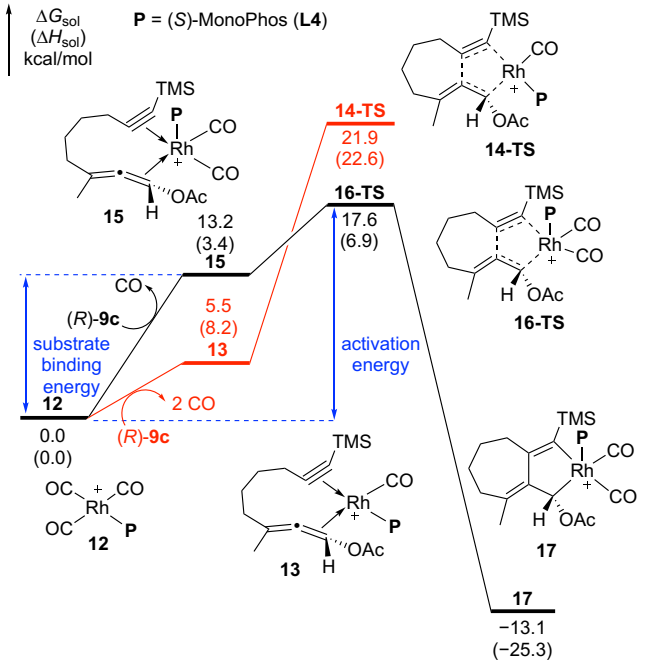

[a] Tetrafluoroborate counteranion is omitted in the calculations.

pect to the resting state **12**. In the alternative pathway shown in black in Scheme 3, allene-yne **9c** replaces one of the CO ligands in **12** to form a square-based pyramidal complex **15**, which is 7.7 kcal/mol less stable than the four-coordinated allene-yne-Rh complex **13**. Nonetheless, the 18-electron complex **15** more readily undergoes oxidative cyclization than the 16-electron complex **13**. The five-coordinated square-based pyramidal oxidative cyclization transition state **16-TS** from **15** is significantly more stable than the four-coordinated **14-TS**. The additional CO ligand stabilizes **16-TS** and decreases the overall activation energy to 17.6 kcal/mol with respect to **12**. The formation of rhodacycle intermediate **17** is highly exothermic. The transition states of subsequent CO insertion and C–C reductive elimination to form the cyclopentenone product are both lower in energy than **16-TS** (see SI for the computed reaction energy profile of the complete catalytic cycle). Thus, the oxidative cyclization is irreversible and enantioselectivity-determining. These mechanistic insights were leveraged computationally to understand the origin of the enantioselectivity obtained using the monodentate phosphoramidite ligand (*S*)-MonoPhos (**L4**).

To investigate the effects of (*S*)-MonoPhos (**L4**) on enantioselectivity and to gain insights for the rational prediction of a more selective ligand, we performed a thorough analysis of the possible transition state isomers leading to both (*R*) and (*S*)-cyclopentenone products. A systematic conformational search of the oxidative cyclization transition states revealed six transition state isomers in the reaction with (*R*)-**9c** to form (*R*)-**10c**: the (*S*)-MonoPhos (**L4**) ligand may occupy any of the three available coordination sites on the Rh and the ligand itself may adopt two different conformations via rotation about the P–Rh bond (Figure 3, **16-TS**, **18-TS**, **19-TS**, **16-TSrot**, **18-TSrot**, and **19-TSrot**). Similarly, when the Rh catalyst reacts with the other enantiomer of the allene-yne to form (*S*)- **10c**, another six transition state isomers were located (**20-TS**, **21-TS**, **22-TS**, **20-TSrot**, **21-TSrot**, and **22-TSrot**). The lowest-energy transition state structures leading to the (*R*)- and (*S*)-products (**16-TS** and **21-TSrot**, respectively) only differ in energy by 1.0 kcal/mol. This small energy difference among transition state isomers agrees with the poor enantioselectivity that is observed experimentally in the APKR with this ligand. These theoretical insights prompted us to explore different strategies to reduce the conformational flexibility of the oxidative cyclization transition states and optimize the catalyst-substrate steric interactions to differentiate the (*R*)- and (*S*)-selective transition states.

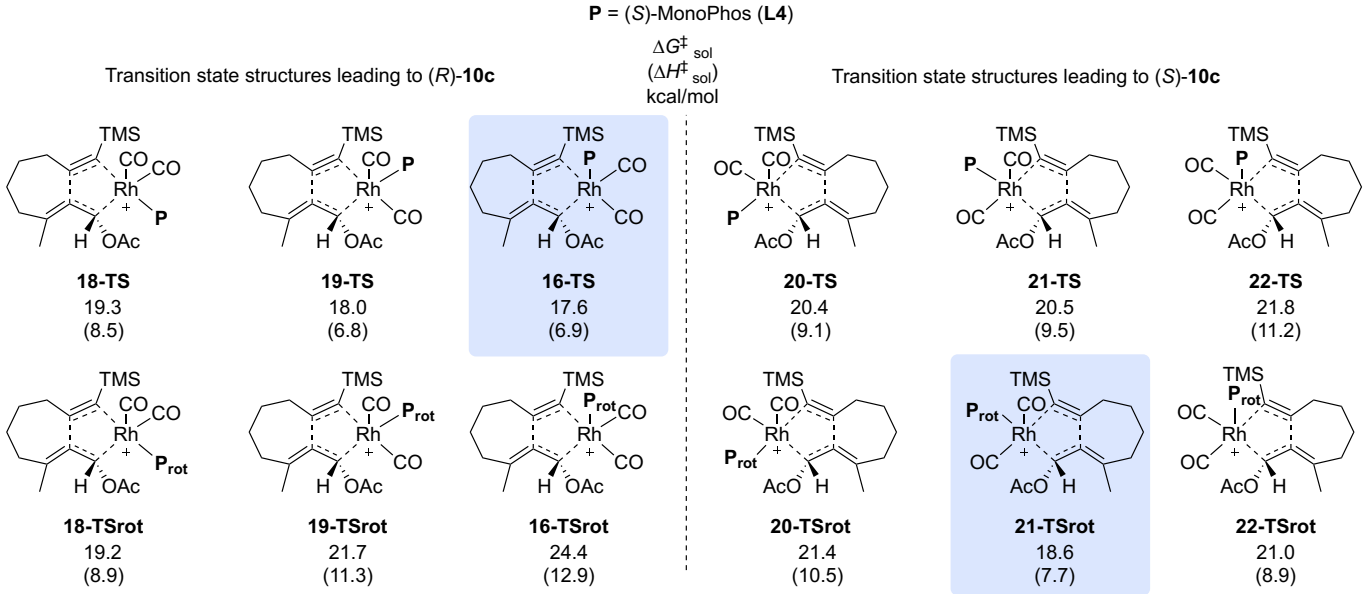

Figure 3. APKR transition state isomers using (*S*)-MonoPhos (**L4**). P_{rot} designates a different ligand conformation by rotation about the Rh–P bond. Tetrafluoroborate counteranion is omitted in the calculations.

Table 2. Computationally-guided ligand screening in the asymmetric APKR.

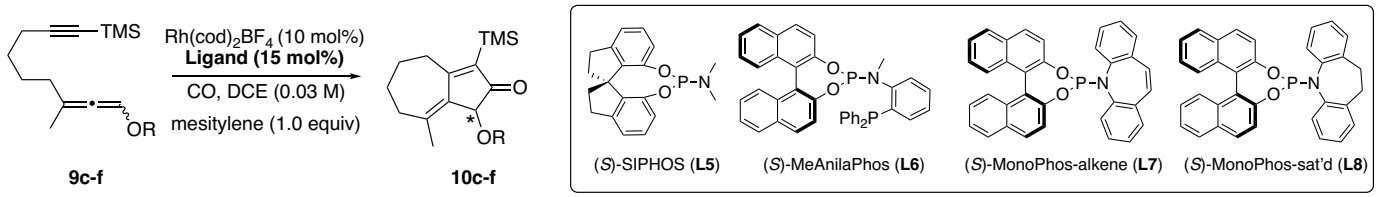

entry	ligand	R	CO (atm)	T (°C)	time (h)	yield (%)[a]	er (*S*:*R*)[b]	$\Delta G^{\ddagger}(S)$[c]	$\Delta G^{\ddagger}(R)$[c]	$\Delta\Delta G^{\ddagger}$[c]
1	**L4**	Ac **9c**	1.0	50	5	**10c** 76	58:42	18.6[d]	17.6[d]	−1.0
2	**L5**	Ac **9c**	1.0	50	10	**10c** 67	29:71	-	-	-
3	**L5**	Piv **9d**	1.0	50	12	**10d** 60	39:61	-	-	-
4	**L6**[e]	Ac **9c**	1.0	50	15	**10c** 18	56:44	26.3[f]	30.7[f]	+4.4
5	**L7**	Ac **9c**	1.0	70	15	**10c** 76	23:77	23.2[f]	18.8[f]	−4.4
6	**L7**	Ac **9c**	0.1	70	15	**10c** 71	18:82	-	-	-
7	**L7**[g]	Ac **9c**	0.1	70	20	**10c** 79[h]	18:82	-	-	-
8	**L7**	Piv **9d**	0.1	70	15	**10d** 50	14:86	-	-	-
9	**L7**	$CO(CH_2)_6CH_3$ **9e**	0.1	70	17	**10e** 70	20:80	-	-	-
10	**L7**	Bz **9f**	0.1	70	20	**10f** 77	15:85	-	-	-
11	**L8**	Ac **9c**	0.1	70	15	**10c** 90	33:67	-	-	-

[a] Reactions were performed on a 0.05 mmol (13-17 mg) scale. Yields were determined by ^{1}H-NMR integration versus mesitylene standard. [b] Enantiomeric ratios were determined by HPLC using a chiral stationary phase. Absolute configurations are assigned by analogy to crystal structure of benzoate **10f** (Figure 6). [c] All energies are in kcal/mol. [d] See Figure 3 for activation energies of all computed transition state isomers. [e] $Rh(cod)_2BF_4$ (5 mol%), **L6** (6 mol%). [f] See SI for activation energies of all computed transition state isomers. [g] Performed on 0.19 mmol (50 mg) scale with 5.0 equiv mesitylene. [h] Isolated yield is reported.

Improving enantioselectivity by modifying the phosphoramidite scaffold. Our first strategy toward improving the enantioselectivity of the APKR was to experimentally test a ligand that is expected to have more significant steric interactions with the substrate in the calculated oxidative transition states shown in Figure 3. Spirocyclic ligand (*S*)-SIPHOS (**L5**), which has previously been applied in the asymmetric PKR of tethered enynes, has a wider "cone angle" than (*S*)-MonoPhos (**L4**).[28] This ligand provided a good yield and, indeed, improved enantioselectivity (29:71 er, Table 2, entry 2). This supports the hypothesis that enhanced ligand-substrate steric interactions are beneficial for enantiocontrol. However, efforts to further improve the selectivity using (*S*)-SIPHOS (**L5**) were unsuccessful. For example, in order to exaggerate the steric interactions between (*S*)-SIPHOS (**L5**) and the acetate group of the substrate, allenyl pivalate **9d** was submitted to the APKR conditions (Table 2, entry 3). The reaction was slowed and the enantioselectivity decreased to 39:61 er. These results imply that simply improving the steric bulk of the monodentate phosphoramidite can only modestly improve the enantioselectivity, as the (*S*)-SIPHOS (**L5**) ligand may still occupy any of the three available binding sites on the Rh center and the facile rearrangement of the ligand minimizes the steric interactions between the ligand and the substrate. We hypothesize that the decrease in enantioselectivity using (*S*)-SIPHOS (**L5**) and pivalate **9d** is due to the decreased binding energy of the (*S*)-SIPHOS (**L5**) ligand that potentially leads to the replacement of (*S*)-SIPHOS (**L5**) with CO in the oxidative cyclization transition state. Taken together, the experimental and computational results for (*S*)-MonoPhos (**L4**) and (*S*)-SIPHOS (**L5**) indicate that although monodentate phosphoramidite ligands provide desired reactivity in the APKR, modification of the steric environment afforded only marginal increases in the enantioselectivity. A strategy to minimize the conformational flexibility of the phosphoramidite ligand is needed. Our second strategy toward improving selectivity was incorporation of chelating ligands to prevent catalyst rearrangement and enhance stereocontrol. In this regard, hybrid *bidentate* phosphine-phosphoramidite ligands have proven advantageous in Rh-catalyzed asymmetric hydroformylation reactions.[28] Therefore, allene-yne **9c** was experimentally tested in the APKR using the bidentate (*S*)-MeAnilaPhos ligand (**L6**).[30] This reaction afforded cyclopentenone product **10c** in only 18% yield and 56:44 er (Table 2, entry 4). Byproduct α,β-unsaturated aldehyde **11c** (Table 1) was obtained in 31% yield. Despite the low yield of **10c** with this ligand, important information was extracted regarding ligand effects on catalyst reactivity by computationally exploring the reaction energy profile using DFT calculations (Scheme 4, see SI for all transition state isomers in reactions with both enantiomers of **9c**). Similar to the reaction with monodentate phosphoramidite ligands, the resting state of the catalyst bearing the bidentate (*S*)-MeAnilaPhos ligand (**L6**) is the four-coordinated square-planar complex **23**. The oxidative cyclization pathways involving both four- and five-coordinated Rh complexes were considered computationally. Coordination of allene-yne **9c** to replace two CO ligands in **23** requires 20.3 kcal/mol to afford the four-coordinated substrate complex **24**. Oxidative cyclization of **24** via **25-TS** requires a very high barrier of 36.0 kcal/mol with respect to **23**. Alternatively, exchanging one of the CO ligands in **23** with allene-yne **9c** yields a five-coordinated square-based pyramidal complex **26** with one CO ligand in the apical position. The unfavorable substrate binding energy of 22.4 kcal/mol indicates that the sterically demanding bidentate ligand prohibits the allene-yne from binding to Rh in a bidentate fashion to effect oxidative cyclization. Similar to the reaction with the monodentate (*S*)-MonoPhos (**L4**) ligand, the oxidative cyclization of the 18-electron complex **26** (via **27-TS**) is more facile than the oxidative cyclization of the 16-electron complex **24**. Nonetheless, the most favorable oxidative cyclization pathway with the (*S*)-MeAnilaPhos (**L6**) ligand still requires a high activation free energy of 26.3 kcal/mol with respect to the catalyst resting

state **23**. This is significantly less favorable than the oxidative cyclization of the same substrate with the (*S*)-MonoPhos (**L4**)-based Rh catalyst ($\Delta G^{\ddagger}$ = 17.6 kcal/mol, see Scheme 3). These results suggest that undesired side reactions may compete with the oxidative cyclization process with the Rh-(*S*)-MeAnilaPhos (**L6**) catalyst and thus lead to the low yield of the APKR products. Isolation of aldehyde **11c** as a major product of this reaction suggests that only the allene moiety is coordinating to the Rh catalyst. Taken together, the above experimental and computational investigations clearly revealed the important role of phosphoramidite ligands on the reactivity and enantioselectivity–cationic Rh(I) catalysts bearing monodentate ligands (*S*)-MonoPhos (**L4**) and (*S*)-SIPHOS (**L5**) are reactive but poorly enantioselective due to the conformational flexibility of the oxidative cyclization transition states with these ligands. In contrast, reactions with the bidentate phosphine-phosphoramidite ligand (*S*)-MeAnilaPhos (**L6**) are not productive due to the unfavorable substrate binding.

Scheme 4. Computed reaction energy profile of the cationic Rh-(*S*)-MeAnilaPhos (L6)-catalyzed APKR.[a]

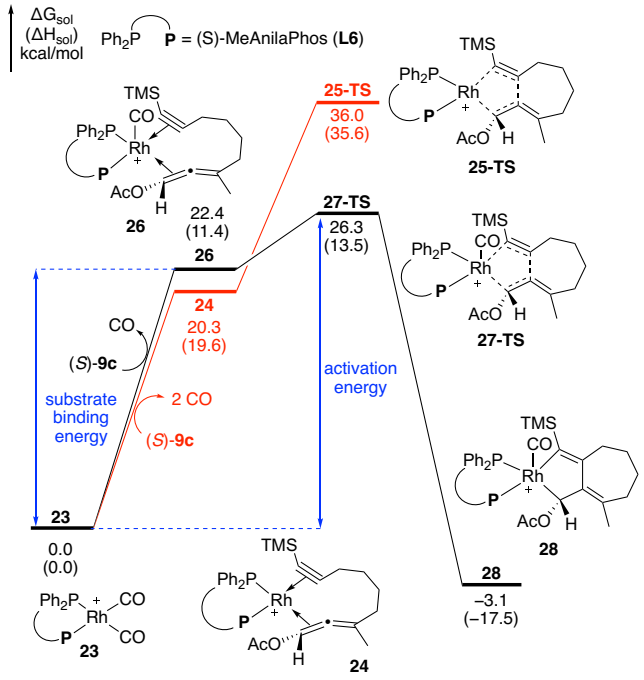

[a] Tetrafluoroborate counteranion is omitted in the calculations.

Balancing reactivity and enantioselectivity using hemilabile bidentate ligand (*S*)-MonoPhos-alkene (L7). In order to increase both the enantioselectivity and reactivity of the APKR, we applied a *hemilabile bidentate* ligand (*S*)-MonoPhos-alkene (**L7**).[31] (*S*)-MonoPhos-alkene (**L7**) was synthesized (see SI) and applied in the APKR to afford product **10c** in 76% yield and 23:77 er (Table 2, entry 5). This high yield combined with improved enantioselectivity inspired further reaction optimization. The reaction proved sensitive to solvent, CO pressure, temperature, additives and scale. For example, when the CO concentration was lowered to 0.1 atm (balloon of 10% gas mixture of CO/Ar), the selectivity improved to 18:82 er (Table 2, entry 6). Incorporation of mesitylene as an additive was necessary for good yields in the APKR. For example, the yield of the APKR of allenyl acetate **9c** improved from 49 to 76% when 1.0 equiv mesitylene was added (see SI). Further details regarding optimization studies can be found in the SI.

The yield of the asymmetric APKR was sensitive to scale. For example, when the reaction was performed using 13 mg of precursor **9c** in an 8-mL test tube, product **10c** was obtained in 71% yield (Table 2, entry 6). However, when 50 mg of the same precursor was used under identical conditions, **10c** was obtained in 41% yield (see SI). By changing a variety of reaction conditions (CO pressure, reaction vessel, and mesitylene equivalents), we discovered that increasing the equivalents of mesitylene from 1.0 to 5.0 gave a yield for the larger scale reaction that was consistent with that of the smaller scale reaction (79%, 18:82 er, entry 7). We attribute this result to the ability of the mesitylene additive to stabilize the cationic Rh catalyst.[32]

Several substrates differing by their acyloxy substituents were submitted to the optimized reaction conditions. Incorporation of a sterically bulky pivaloyloxy group in allene **9d** resulted in an increased er (14:86), but afforded a lower yielding APKR (50%, compare entries 6 and 8). Allenyl octanoate **9e** reacted in similar yield (70%) and enantioselectivity (20:80 er) as **9c** (compare entries 6 and 9). Reaction of allenyl benzoate **9f** afforded the APKR product **10f** in 77% yield and 15:85 er (entry 10). Substrate **9g**, functionalized with an electron-withdrawing *p*-nitrobenzoyl group, afforded the APKR product **10g** in 45% yield and 23:77 er (see SI).

Experimental evidence for Type I DyKAT mechanism. Experiments were conducted to test whether the observed enantioselectivity was arising from a dynamic kinetic resolution (DKR), Type I DyKAT, or Type II DyKAT mechanism.[13] Ph-substituted alkyne **9a** was chosen as a substrate for these experiments because its enantiomers were readily resolved by HPLC using a chiral stationary phase. Single enantiomers of allenyl acetate **9a** were isolated and subjected to the APKR reaction conditions (Scheme 5, reaction 1). After 30 min, the allenyl acetates had completely racemized, and no evidence of APKR product **10a** was observed. Therefore, allenyl acetate racemization is faster than the APKR. Regardless of which

Scheme 5. Experiments supporting Type I DyKAT mechanism.[a,b]

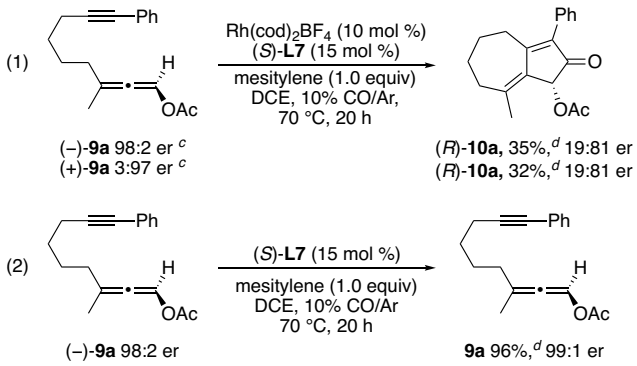

[a] Reactions were performed using 3.5 mg each of allenyl acetate starting material. [b] Enantiomeric ratios were determined by HPLC using a chiral stationary phase. [c] Complete racemization (50:50 er) observed after 30 min. [d] Yields were determined by ^{1}H-NMR integration versus mesitylene standard.

allene enantiomer was reacted, the same product (*R*)-**10a** was obtained after 20 h. Thus, enantioselectivity is catalyst-controlled, and is established during the APKR. The low yields of these reactions

are attributed to the small scale of the experiments (3.5 mg each). In an additional experiment, a single enantiomer of (−)-**9a** was subjected to the reaction conditions without the Rh catalyst. The allene was recovered (96%) and no scrambling of axial chirality was observed, supporting the hypothesis that allene isomerization is catalyzed by Rh (Scheme 5, reaction 2). Taken together, the results of these mechanistic studies support catalyst-controlled enantioselectivity enabled by rapid, Rh-catalyzed allenyl acetate isomerization. Therefore, the enantioselective APKR of allenyl acetates is classified as Type I DyKAT.

Computational and experimental investigation of the mechanism and origin of enantioselectivity in the APKR with (*S*)-MonoPhos-alkene (L7). Although the Rh is expected to adopt a five-coordinated square-based pyramidal geometry in the oxidative cyclization, two different pathways involving the alkene group of the ligand **L7** either bound or unbound to the Rh are possible. To elucidate the most preferred pathway in the enantio-determining oxidative cyclization step, both *alkene bound* and *unbound* pathways were investigated using DFT calculations (Scheme 6). In both pathways, the resting state of the catalyst is the square planar complex **30** that exists in equilibrium with alkene-bound complex **29**, which is 8.7 kcal/mol higher in energy. The hemilabile nature of the (*S*)-MonoPhos-alkene (**L7**) ligand in **29** and **30** indicates a Curtin-Hammett system in which the exact mechanism of oxidative cyclization is determined by the energy difference of the oxidative cyclization transition states. In the *alkene unbound* pathway (Scheme 6, left), coordination of the allene-yne **9c** affords five-coordinated substrate complex **31**, in which the Rh is coordinated with two CO ligands and the hemilabile (*S*)-MonoPhos-alkene (**L7**) in a monodentate fashion. Formation of the diastereomeric complexes (*R*)- and (*S*)-**31**, in which the Rh binds to (*R*)- and (*S*)-**9c**, respectively, require substrate binding energies of 12.0 and 18.4 kcal/mol with respect to **30**. In this *alkene unbound* APKR pathway, the oxidative cyclization of (*R*)-**9c** via (*R*)-**32-TS** requires a 4.4 kcal/mol lower activation free energy than the reaction with (*S*)-**9c** via (*S*)-**32-TS**. This energy difference predicts the enantioselective formation of the APKR product (*R*)-**10c**

In the alternative *alkene bound* pathway (Scheme 6, right), the oxidative cyclization occurs via five-coordinated square-based pyramidal transition states (*R*)- and (*S*)-**35-TS** bearing only one CO ligand and the hemilabile (*S*)-MonoPhos-alkene (**L7**) ligand bound in a bidentate fashion. Interestingly, the substrate complexes (*R*)- and (*S*)-**34** in this one-CO pathway remain four-coordinated with the alkene unbound from the Rh center. This result is consistent with the reaction profiles of mono- and bidentate ligands **L4** and **L6** that the 16-electron four-coordinated Rh(I) reactant complexes are more stable than the 18-electron complexes (see Schemes 3 and 4). The formation of the four-coordinated reactant complexes (*R*)- and (*S*)-**34** are also facile with low substrate binding energies. However, these 16-electron species are less reactive than the 18-electron complexes (*R*)- and (*S*)-**31** in the oxidative cyclization. The *alkene bound*, one-CO pathway has a higher overall activation energy ($\Delta G^{\ddagger}$ = 23.6 kcal/mol, (*S*)-**35-TS**) than the *alkene unbound* pathway ($\Delta G^{\ddagger}$ = 18.8 kcal/mol, (*R*)-**32-TS**). In summary, DFT calculations predict that the APKR with (*S*)-MonoPhos-alkene (**L7**) occurs via the *alkene unbound* pathway and affords (*R*)-**10c**.

Scheme 6. Computed reaction energy profile of the cationic Rh-(*S*)-MonoPhos-alkene (L7)-catalyzed APKR.[a]

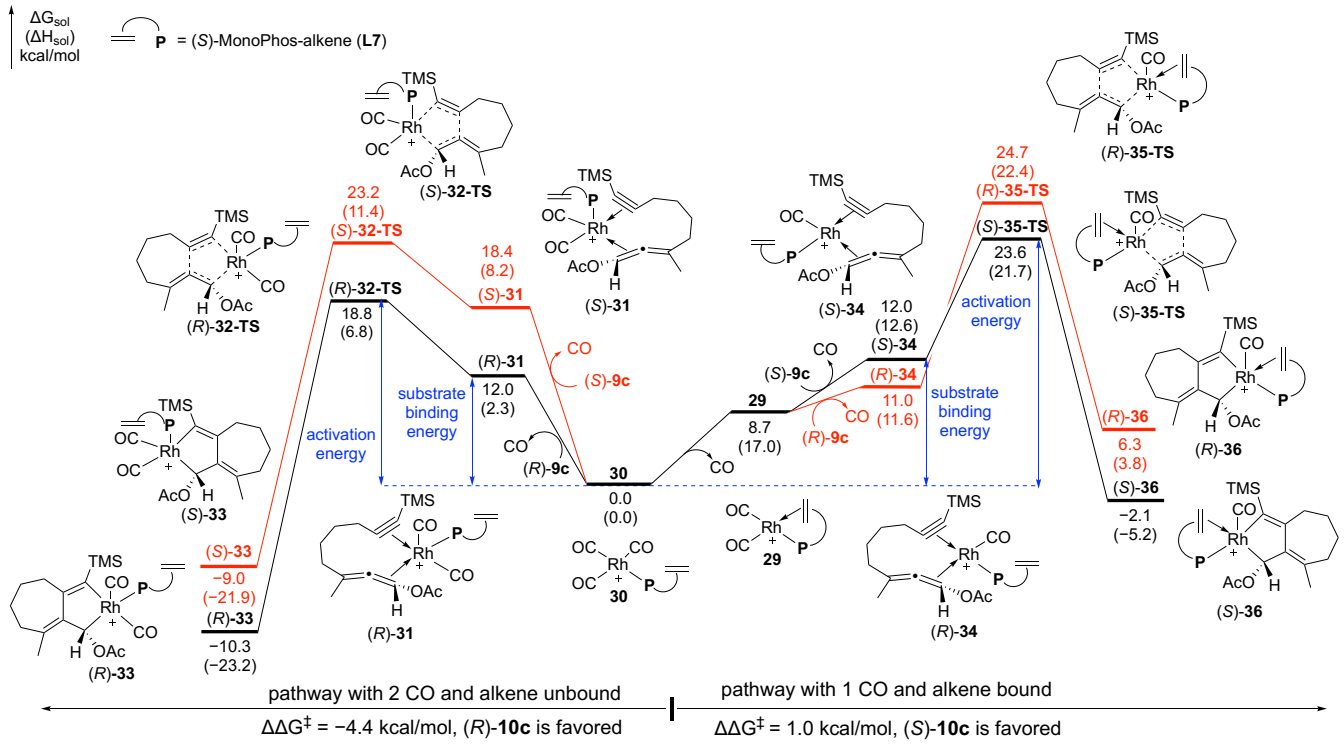

[a] Tetrafluoroborate counteranion is omitted in the calculations.

Experimental validation of *alkene unbound* pathway and predicted absolute configuration of the major product. To experimentally test whether the reaction proceeds via the *alkene unbound* pathway, saturated ligand **L8** was applied in the APKR. The reac-

tion of **9c** using (*S*)-MonoPhos-sat'd (**L8**) ligand provided **10c** in 90% yield and 33:67 er, with the same major enantiomeric product as that obtained with **L7** (Table 2, entry 7). This result suggests that the alkene in **L7** is unbound in the oxidative cyclization transition state, as predicted by DFT calculations (Scheme 6). The higher enantioselectivity with phosphoramidite-alkene ligand **L7** suggests that the hemilability of the ligand plays a key role in achieving a high level of enantiocontrol by preventing rearrangement or dissociation of the ligand.

Calculations with (*S*)-MonoPhos-alkene (**L7**) predict that the (*R*) absolute configuration of APKR product **10c** is preferred (Scheme 6). To test this computational prediction experimentally, the APKR was performed on allene-yne **9f** to give benzoate **10f** as an amorphous white solid (77% yield, 15:85 er, Table 2, entry 10). After two recrystallizations in pentane, the enantiopurity of **10f** was enhanced to 2:98 er. An X-ray quality crystal was grown by slow cooling in hexanes. The absolute configuration of benzoate **10f** was unambiguously assigned as (*R*) by X-ray crystallography (Figure 4). Therefore, we assign the absolute configuration of acetate product **10c** as (*R*), based on analogous HPLC retention times of the major and minor enantiomers. This stereochemical assignment of (*R*)-**10c** matches that predicted by computation (Scheme 6).

Origin of enantioselectivity of (*S*)-MonoPhos-alkene ligand (L7). In the favorable *alkene unbound* APKR pathway, six different oxidative cyclization transition state isomers are possible in the reaction with each enantiomer of allene-yne **9c**. We calculated the activation energies of all 12 transition state isomers using the (*S*)-MonoPhos-alkene (**L7**) ligand to determine the origin of enantioselectivity. The two lowest-energy transition states in the reaction with each enantiomer are shown in Figure 5 (see SI for other higher-energy transition state isomers). The two lowest-energy transition states in the reaction with (*R*)-**9c** that lead to (*R*)-**10c** ($\Delta G^{\ddagger}$ = 18.8 and 19.8 kcal/mol) are both much more stable than the lowest-energy transition states in the reaction with (*S*)-**9c** that forms (*S*)-**10c** ($\Delta G^{\ddagger}$ = 23.2 and 24.6 kcal/mol). Here, the DFT-calculations predicted much greater enantioselectivity ($\Delta\Delta G^{\ddagger}$ = 4.4 kcal/mol) than that observed experimentally (18:82 er). Our benchmark calculations suggest the choice of density functional and basis set has minimal effects on the calculated $\Delta\Delta G^{\ddagger}$ value (see SI for details). Thus, we hypothesize the lower enantioselectivity observed experimentally may be affected by experimental conditions, such as counteranions, mesitylene additives, which were not considered in the DFT calculations.

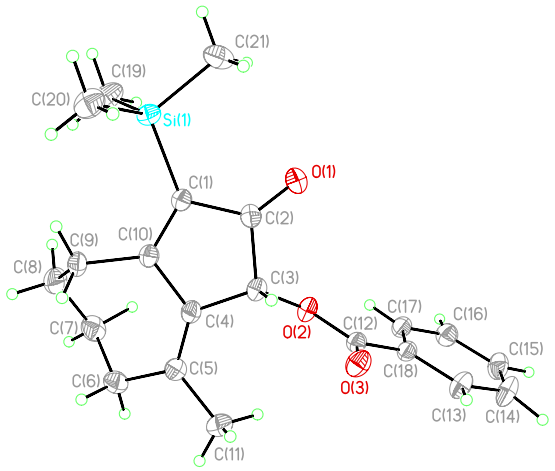

Figure 4. Crystal structure of (*R*)-**10f**.

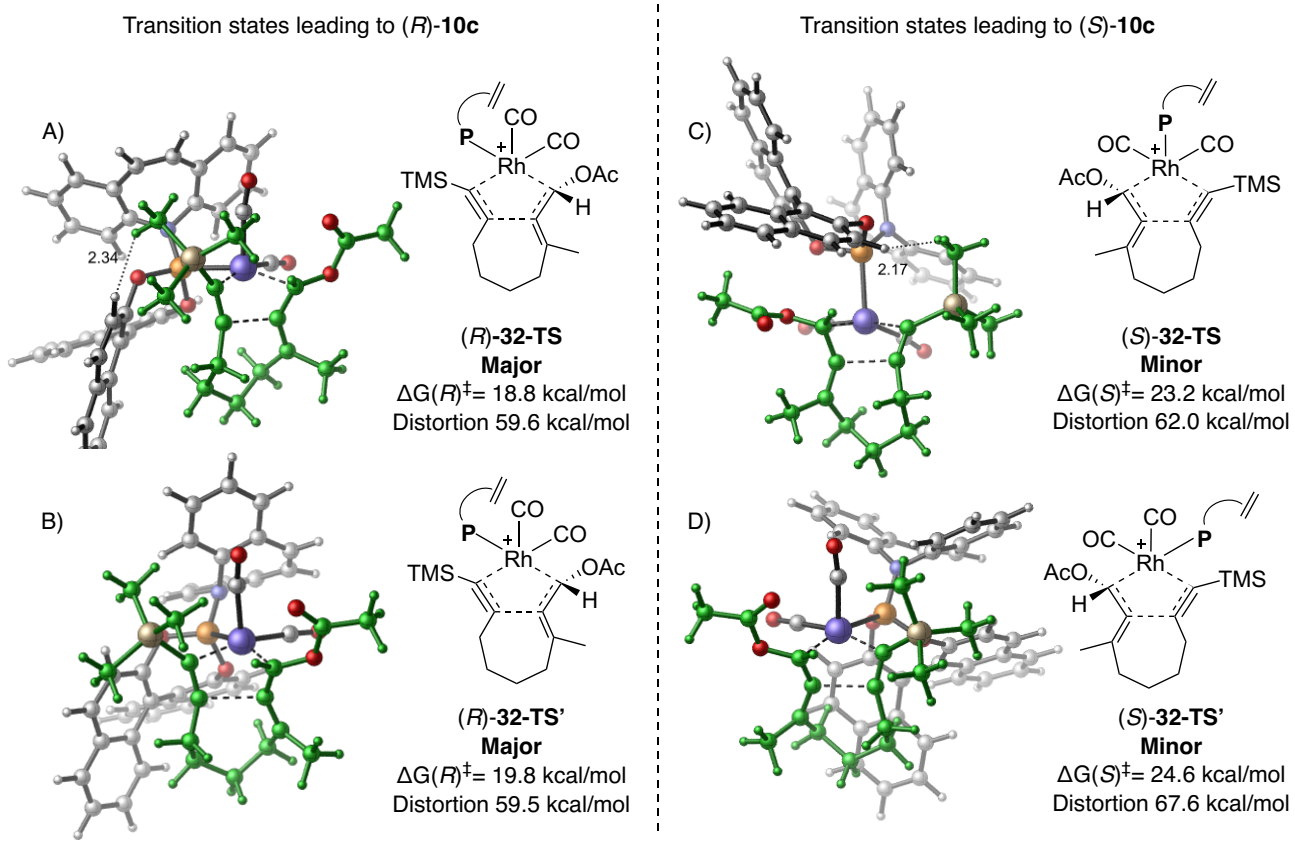

Figure 5. Lowest-energy oxidative cyclization transition state isomers of APKR with (*S*)-MonoPhos-alkene ligand (**L7**). The allene-yne substrate is highlighted in green. Rh is in blue and phosphorous is in orange.

To explore the origin of the enantioselectivity, we calculated the distortion energies of the ligand and the substrate in the oxidative cyclization transition states.[33] The distortion energy represents the total energy required for the (*S*)-MonoPhos-alkene ligand (**L7**) and the allene-yne substrate to adopt their respective transition state geometries from the undistorted ground state conformation (see SI for details). The relative distortion energies $\Delta\Delta E_{dist}$ with respect to the least-distorted transition state (*R*)-**32-TS** are shown in Figure 5. The two lowest-energy transition states leading to (*R*)-**10c** (Figure 5A and 5B) have significantly lower total distortion energies than the two lowest-energy transition states leading to (*S*)-**10c** (5C and 5D). Other higher-energy transition state isomers suffer even greater distortion energies (See SI for details). These results indicate the higher barriers in the pathways to form the minor enantiomer (*S*)-**10c** are due to the unfavorable steric repulsions between the substrate and ligand **L7**. In (*S*)-**32-TS**, one steric interaction that is easily identified is between the binaphthyl backbone of the ligand and the TMS group of the substrate, which is evidenced by the short H…H distance (2.17 Å) between the TMS and the binaphthyl group. In comparison, in the lowest-energy transition state leading to (*R*)-**10c** (Figure 5A), the distance between these two groups is much longer (2.34 Å). The second lowest energy transition state isomer that leads to (*S*)-**10c** (Figure 5D) is destabilized by an unfavorable steric repulsion between the forming seven-membered ring and the binaphthyl moiety on the ligand.

Summary of ligand effects on reactivity and enantioselectivity. The computed activation free energies in the enantioselectivity-determining oxidative cyclization step of the APKR of **9c** with three different ligands (**L4**, **L6**, and **L7**) are summarized in Figure 6. For each reaction, multiple transition state

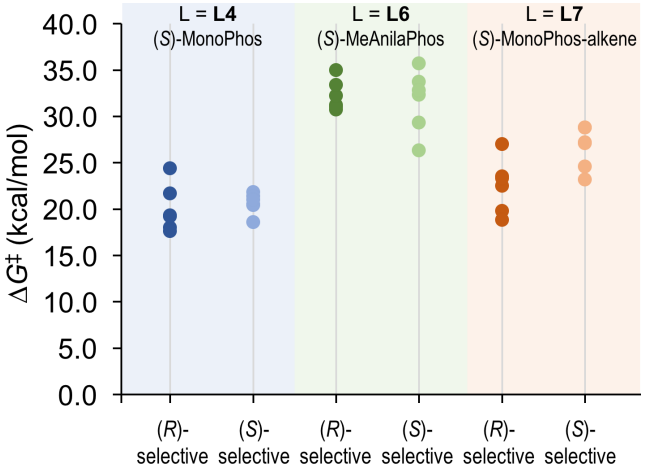

Figure 6. Summary of computed activation energies of the oxidative cyclization transition state isomers in the Rh-catalyzed APKR reactions of allene-yne (*R*)- and (*S*)-**9c** with different ligands. (*R*)-selective transition state isomers are in the reaction with (*R*)-**9c** and form (*R*)-**10c**. (*S*)-selective transition state isomers are in the reaction with (*S*)-9c and form (*S*)-**10c**.

isomers are located within a few kcal/mol, indicating the importance of the systematic conformational search to locate all possible transition state isomers in the computational prediction of enantioselectivity. The DFT calculations revealed significant effects of the phosphoramidite ligands on both reactivity and selectivity. While most of the transition state isomers with (*S*)-MonoPhos (**L4**) have very similar activation free energies in the (*R*)- and (*S*)-selective pathways, the (*R*)-selective transition state isomers with the (*S*)-MonoPhos-alkene (**L7**) ligand are noticeably more stable than the (*S*)-selective transition states. Both the (*R*)- and (*S*)-selective pathways with the bidentate (*S*)-MeAnilaPhos (**L6**) ligand require high activation energy, indicating the low APKR reactivity of this class of ligand.

CONCLUSIONS

The asymmetric APKR of allenyl acetates represents the first example of a DyKAT carbonylation reaction, the first catalyst-controlled enantioselective PKR of an allene, and a rare example of a DyKAT of an allene. A reactive and enantioselective catalyst was designed through a unique combination of DFT studies and laboratory experiments. Once phosphoramidites were identified as a reactive ligand class, mechanistic information provided by computation enabled us to achieve good enantioselectivity (14:86 er) after experimentation with only four different phosphoramidite ligands, demonstrating the power of computation in streamlining the selection of chiral ligands. The computational study addressed a series of mechanistic questions that are critical for the proper prediction of ligand effects on reactivity and enantioselectivity of APKR, including facile catalyst rearrangement, the number of CO ligands bound to the Rh center, and the binding mode of a hemilabile phosphoramidite ligand. After obtaining these mechanistic insights, the calculated reactivity and selectivity ($\Delta G^{\ddagger}$ and $\Delta\Delta G^{\ddagger}$) were used as a guide to understand the experimental yield and er and to make rational prediction of a more selective and reactive ligand. The enantioselectivity of hemilabile (*S*)-MonoPhos-alkene (**L7**) was accurately predicted by computation and the absolute configuration of the major enantiomer was corroborated by X-ray crystallography.

Computational tools are rapidly developing toward being able to predict enantioselective catalysts *in silico*. However, the present study accentuated the challenges in the practical application of computational ligand design. A simple "brute-force"-type screening of the relative energies of enantioselectivity-determining transition states is often not sufficient, as the modification of ligand denticity and structure may lead to significant change in the reaction mechanism. The present study offers an informed approach through close collaboration of experimental and computational chemists to achieve rational ligand design with greater efficiency and reliability. This iterative experimental and computational approach to catalyst design enables real-time updates and validation to the computational predictions which in turn can be immediately used to inform the next generation of experiments.

ASSOCIATED CONTENT

Supporting Information

The Supporting Information is available free of charge on the ACS Publications website.

Detailed experimental procedures and characterization data for all new compounds, HPLC traces of compounds **10a-g** (PDF)

X-ray crystallographic data for compound **10f** (CIF). The crystallographic data is deposited with the Cambridge Structural Database under Reference No. CCDC 1547487.

Computational details and Cartesian coordinates of optimized geometries (PDF)

AUTHOR INFORMATION

Corresponding Author

* kbrummon@pitt.edu, pengliu@pitt.edu

ACKNOWLEDGMENT

We thank the NIH (GM-54161) and the NSF (CHE-1654122) for funding. Calculations were performed at the Center for Research Computing at the University of Pittsburgh and the Extreme Science and Engineering Discovery Environment (XSEDE) supported by NSF.

REFERENCES

(1) (a) Brady, S. F.; Singh, M. P.; Janso, J. E.; Clardy, J., *J. Am. Chem. Soc.* **2000**, *122*, 2116-2117. (b) Zhao, Y.-M.; Gu, P.; Tu, Y.-Q.; Fan, C.-A.; Zhang, Q., *Org. Lett.* **2008**, *10*, 1763-1766. (c) Castro, V.; Murillo, R.; Klaas, C. A.; Meunier, C.; Mora, G.; Pahl, H. L.; Merfort, I., *Planta Med.* **2000**, *66*, 591-595. (d) Wang, Q.; Chen, T.-H.; Bastow, K. F.; Morris-Natschke, S. L.; Lee, K.-H.; Chen, D.-F., *J. Nat. Prod.* **2013**, *76*, 305-310.
(2) (a) Wender, P. A.; Jesudason, C. D.; Nakahira, H.; Tamura, N.; Tebbe, A. L.; Ueno, Y., *J. Am. Chem. Soc.* **1997**, *119*, 12976-12977. (b) Urabe, D.; Asaba, T.; Inoue, M., *Bull. Chem. Soc. Jpn.* **2016**, *89*, 1137-1144. (c) Hao, H.-D.; Trauner, D., *J. Am. Chem. Soc.* **2017**, *139*, 4117-4122. (d) Xu, G.; Hou, A.-J.; Zheng, Y.-T.; Zhao, Y.; Li, X.-L.; Peng, L.-Y.; Zhao, Q.-S., *Org. Lett.* **2006**, *9*, 291-293. (e) Zhang, Y.; Di, Y.; He, H.; Li, S.; Lu, Y.; Gong, N.; Hao, X., *Eur. J. Org. Chem.* **2011**, *2011*, 4103-4107.
(3) (a) Xu, C.; Han, A.; Virgil, S. C.; Reisman, S. E., *ACS Cent. Sci.* **2017**, *3*, 278-282. (b) Ren, F.; Hogan, P. C.; Anderson, A. J.; Myers, A. G., *J. Am. Chem. Soc.* **2007**, *129*, 5381-5383. (c) Moser, B. R., *J. Nat. Prod.* **2008**, *71*, 487-491. (d) Murakami, N.; Ye, Y.; Kawanishi, M.; Aoki, S.; Kudo, N.; Yoshida, M.; Nakayama, E. E.; Shioda, T.; Kobayashi, M., *Bioorg. Med. Chem. Lett.* **2002**, *12*, 2807-2810. (e) Abd El-Gaber, M. K.; Yasuda, S.; Iida, E.; Mukai, C., *Org Lett.* **2017**, *19*, 320-323.
(4) Chen, B.-C.; Zhou, P.; Davis, F. A.; Ciganek, E., *Organic Reactions*, John Wiley & Sons, Inc.: **2004**.
(5) (a) Simeonov, S. P.; Nunes, J. P. M.; Guerra, K.; Kurteva, V. B.; Afonso, C. A. M., *Chem. Rev.* **2016**, *116*, 5744-5893. (b) Marín-Barrios, R.; García-Cabeza, A. L.; Moreno-Dorado, F. J.; Guerra, F. M.; Massanet, G. M., *J. Org. Chem.* **2014**, *79*, 6501-6509. (c) Smithen, D. A.; Mathews, C. J.; Tomkinson, N. C. O., *Org. Biomol. Chem.* **2012**, *10*, 3756-3762.
(6) Krautwald, S.; Carreira, E. M., *J. Am. Chem. Soc.* **2017**, *139*, 5627-5639.
(7) Brummond, K. M.; Davis, M. M.; Huang, C., *J. Org. Chem.* **2009**, *74*, 8314-8320.
(8) (a) Grillet, F.; Huang, C.; Brummond, K. M., *Org. Lett.* **2011**, *13*, 6304-6307. (b) Tap, A.; Jouanneau, M.; Galvani, G.; Sorin, G.; Lannou, M.-I.; Férézou, J.-P.; Ardisson, J., *Org. Biomol. Chem.* **2012**, *10*, 8140.
(9) (a) Doan, N. T. Q.; Christensen, S. B., *Curr. Pharm. Des.* **2015**, *21*, 5501-5517. (b) Doan, N. T.; Paulsen, E. S.; Sehgal, P.; Moller, J. V.; Nissen, P.; Denmeade, S. R.; Isaacs, J. T.; Dionne, C. A.; Christensen, S. B., *Steroids* **2015**, *97*, 2-7. (c) Doan, N. T. Q.; Crestey, F.; Olsen, C. E.; Christensen, S. B., *J. Nat. Prod.* **2015**, *78*, 1406-1414. (d) Winther, A.-M. L.; Liu, H.; Sonntag, Y.; Olesen, C.; le Maire, M.; Soehoel, H.; Olsen, C.-E.; Christensen, S. B.; Nissen, P.; Møller, J. V., *J. Biol. Chem.* **2010**, *285*, 28883-28892. (e) Mahalingam, D.; Wilding, G.; Denmeade, S.; Sarantopoulas, J.; Cosgrove, D.; Cetnar, J.; Azad, N.; Bruce, J.; Kurman, M.; Allgood, V. E.; Carducci, M., *Br. J. Cancer* **2016**, *114*, 986-994.
(10) (a) Chu, H.; Smith, J. M.; Felding, J.; Baran, P. S., *ACS Cent. Sci.* **2017**, *3*, 47-51. (b) Chen, D.; Evans, P. A., *J. Am. Chem. Soc.* **2017**, DOI: 10.1021/jacs.7b01734.
(11) We expect that an asymmetric APKR will ultimately enable stereoselective access to C-2 analogs of the bicyclo[5.3.0]decane ring system. For example, despite recent syntheses of Tg by Baran and Evans,[10] to date only four C-2 Tg analogs have been prepared, and when compared to Tg, their activities ranged from ten times more potent to 40 times less potent.[9a] Moreover, naturally occurring Tg analogs which lack a C-2 ester show decreased SERCA binding affinity.[9d]
(12) Jorgensen, L.; McKerrall, S. J.; Kuttruff, C. A.; Ungeheuer, F.; Felding, J.; Baran, P. S., *Science,* **2013**, *341*, 878-882.
(13) Bhat, V.; Welin, E. R.; Guo, X.; Stoltz, B. M., *Chem. Rev.*, **2017**, *117*, 4528-4561
(14) Kim, D. E.; Kim, I. S.; Ratovelomanana-Vidal, V.; Genêt, J.-P.; Jeong, N., *J. Org. Chem.* **2008**, *73*, 7985-7989.
(15) (a) Furusawa, T.; Morimoto, T.; Ikeda, K.; Tanimoto, H.; Nishiyama, Y.; Kakiuchi, K.; Jeong, N., *Tetrahedron,* **2015**, *71*, 875-881. (b) Kwong, F. Y.; Lee, H. W.; Qiu, L.; Lam, W. H.; Li, Y.-M.; Kwong, H. L.; Chan, A. S. C., *Adv. Synth. Catal.* **2005**, *347*, 1750-1754.
(16) Sawano, T.; Thacker, N. C.; Lin, Z. K.; McIsaac, A. R.; Lin, W. B., *J. Am. Chem. Soc.* **2015**, *137*, 12241-12248.
(17) (a) Ricker, J. D.; Geary, L. M., *Topics in Catalysis,* **2017**, DOI: 10.1007/s11244-017-0741-0. (b) Quintero-Duque, S.; Dyballa, K. M.; Fleischer, I., *Tetrahedron Lett.* **2015**, *56*, 2634-2650. (c) Lledó, A.; Verdaguer, X.; Riera, A., *The Pauson-Khand Reaction*, John Wiley & Sons, Ltd. **2012**, 147-180.
(18) (a) Zhang, Z. B.; Bender, C. F.; Widenhoefer, R. A., *J. Am. Chem. Soc.* **2007**, *129*, 14148-14149. (b) Osborne, J. D.; Randell-Sly, H. E.; Currie, G. S.; Cowley, A. R.; Willis, M. C., *J. Am. Chem. Soc.* **2008**, *130*, 17232-17233. (c) Chen, M.; Roush, W. R., *J. Am. Chem. Soc.* **2011**, *133*, 5744-5747. (d) Tran, D. N.; Cramer, N., *Angew. Chem. Int. Ed.* **2013**, *52*, 10630-10634. (e) Trost, B. M.; Fandrick, D. R.; Dinh, D. C., *J. Am. Chem. Soc.* **2005**, *127*, 14186-14187.
(19) Commentaries and tutorial reviews regarding computational catalyst design: (a) Poree, C.; Schoenebeck, F., *Acc. Chem. Res.* **2017,** *50*, 605-608. (b) Peng, Q.; Duarte, F.; Paton, R. S., *Chem. Soc. Rev.* **2016**, *45*, 6093-6107. (c) Sunoj, R. B., *Acc. Chem. Res.* **2016**, *49*, 1019-1028. (d) Houk, K. N.; Cheong, P. H.-Y., *Nature,* **2008**, *455*, 309-313.
(20) Selected examples of transition metal catalysts identified by computation: (a) Straker, R. N.; Peng, Q.; Mekareeya, A.; Paton, R. S.; Anderson, E. A., *Nat. Commun.* **2016**, *7*, 10109. (b) Nielsen, M. C.; Bonney, K. J.; Schoenebeck, F., *Angew. Chem., Int. Ed.* **2014**, *53*, 5903-5906. (c) Doney, A. C.; Rooks, B. J.; Lu, T.; Wheeler, S. E., *ACS Catal.* **2016**, *6*, 7948-7955.
(21) (a) Jeong, N.; Sung, B. K.; Choi, Y. K., *J. Am. Chem. Soc.* **2000**, *122*, 6771-6772. (b) Kim, D. E.; Ratovelomanana-Vidal, V.; Jeong, N., *Adv. Synth. Catal.* **2010**, *352*, 2032-2040.
(22) Gawley, R. E., *J. Org. Chem.* **2006**, *71*, 2411-2416.
(23) Scheffel, D. J.; Cole, A. R.; Jung, D. M.; Schiavelli, M. D., *J. Am. Chem. Soc.* **1980**, *102*, 267-270.
(24) (a) Nelson, D. J.; Nolan, S. P., *Chem. Soc. Rev.* **2013**, *42*, 6723-6753. (b) Voutchkova, A. M.; Appelhans, L. N.; Chianese, A. R.; Crabtree, R. H., *J. Am. Chem. Soc.* **2005**, *127*, 17624-17625.
(25) (a) Rodriguez, A. M.; Prieto, P., *Tetrahedron* **2016**, *72*, 7443-7448. (b) Fager-Jokela, E.; Muuronen, M.; Khaizourane, H.; Vazquez-Romero, A.; Verdaguer, X.; Riera, A.; Helaja, J., *J. Org. Chem.* **2014**, *79*, 10999-11010. (c) Yamanaka, M.; Nakamura, E., *J. Am. Chem. Soc.* **2001**, *123*, 1703-1708.
(26) (a) Baik, M. H.; Mazumder, S.; Ricci, P.; Sawyer, J. R.; Song, Y. G.; Wang, H.; Evans, P. A., *J. Am. Chem. Soc.* **2011**, *133*, 7621-7623. (b) Wang, H.; Sawyer, J. R.; Evans, P. A.; Baik, M. H., *Angew. Chem.* **2008**, *47*, 342-345.
(27) Bayden, A. S.; Brummond, K. M.; Jordan, K. D., *Organometallics,* **2006**, *25*, 5204-5206.
(28) Fan, B. M.; Xie, J. H.; Li, S.; Tu, Y. Q.; Zhou, Q. L., *Adv. Synth. Catal.* **2005**, *347*, 759-762.

(29) (a) Chikkali, S. H.; van der Vlugt, J. I.; Reek, J. N. H., *Coord. Chem. Rev.* **2014**, *262*, 1-15. (b) Franke, R.; Selent, D.; Borner, A., *Chem. Rev.* **2012**, *112*, 5675-5732. (c) Wassenaar, J.; Reek, J. N. H., *Org. Biomol. Chem.* **2011**, *9*, 1704-1713.
(30) Vallianatou, K. A.; Kostas, I. D.; Holz, J.; Borner, A., *Tetrahedron Lett.* **2006**, *47*, 7947-7950.
(31) (a) Rössler, S. L.; Krautwald, S.; Carreira, E. M., *J. Am. Chem. Soc.* **2017**, *139*, 3603-3606. (b) Defieber, C.; Ariger, M. A.; Moriel, P.; Carreira, E. M., *Angew. Chem.* **2007**, *46*, 3139-3143. (c) Drinkel, E.; Briceño, A.; Dorta, R, *Organometallics,* **2010**, *29*, 2503-2514. (d) Bhaskararao, B.; Sunoj, R. B., *J. Am. Chem. Soc.* **2015**, *137*, 15712-15722.
(32) Ojima, I.; Vu, A. T.; Bonafoux, D., *Science of Synthesis*. Thieme Chemistry, **2001**, 531-532.
(33) (a) Bickelhaupt, F. M.; Houk, K. N., *Angew. Chem. Int. Ed.* **2017**, DOI: 10.1002/anie.201701486. (b) Fernandez, I.; Bickelhaupt, F. M., *Chem. Soc. Rev.* **2014**, *43*, 4953-4967. (c) Ess, D. H.; Houk, K. N., *J. Am. Chem. Soc.* **2008**, *130*, 10187-10198.

SYNOPSIS TOC

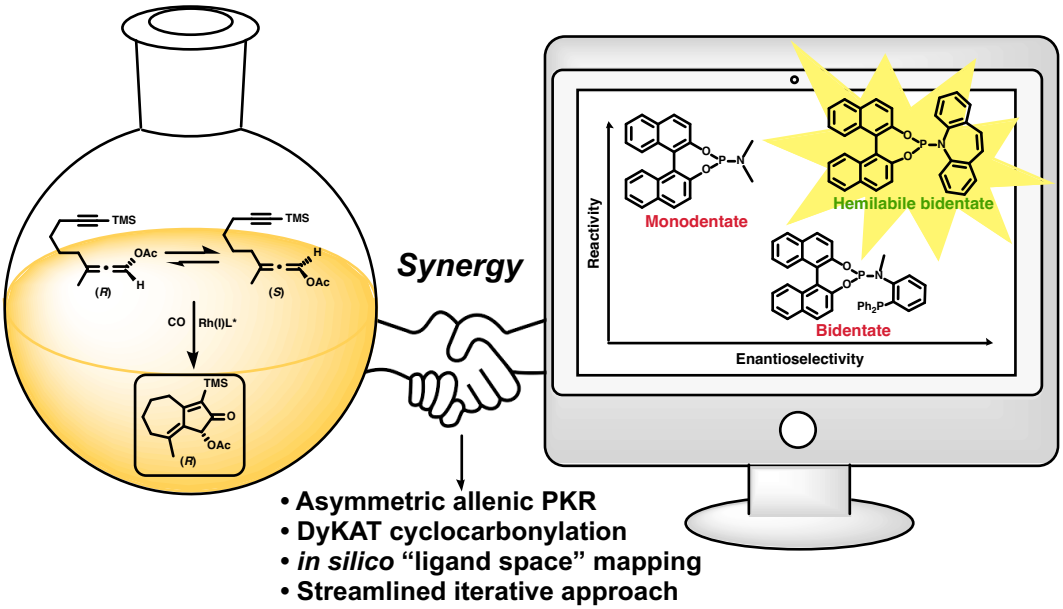

• **Asymmetric allenic PKR**
• **DyKAT cyclocarbonylation**
• ***in silico* "ligand space" mapping**
• **Streamlined iterative approach**

.